Dendritic action potentials connect distributed dendrodendritic microcircuits

M. Migliore · Gordon M. Shepherd

Abstract Lateral inhibition of cells surrounding an excited area is a key property of sensory systems, sharpening the preferential tuning of individual cells in the presence of closely related input signals. In the olfactory pathway, a dendrodendritic synaptic microcircuit between mitral and granule cells in the olfactory bulb has been proposed to mediate this type of interaction through granule cell inhibition of surrounding mitral cells. However, it is becoming evident that odor inputs result in broad activation of the olfactory bulb with interactions that go beyond neighboring cells. Using a realistic modeling approach we show how backpropagating action potentials in the long lateral dendrites of mitral cells, together with granule cell actions on mitral cells within narrow columns forming glomerular units, can provide a mechanism to activate strong local inhibition between arbitrarily distant mitral cells. The simulations predict a new role for the dendro-dendritic synapses in the multicolumnar organization of the granule cells. This new paradigm gives insight into the functional significance of the patterns of connectivity revealed by recent viral tracing studies. Together they suggest a functional wiring of the olfactory bulb that could greatly expand the computational roles of the mitral–granule cell network.

Action Editor: Alain Destexhe

M. Migliore · G. M. Shepherd
Department of Neurobiology, Yale University School
of Medicine, New Haven, CT, USA

M. Migliore (✉)
Institute of Biophysics, National Research Council,
via U. La Malfa 153, 90146 Palermo, Italy
e-mail: michele.migliore@pa.ibf.cnr.it, michele.migliore@yale.edu

1 Introduction

Lateral inhibition plays a central role in processing sensory information in most sensory systems. Its most obvious role is in the visual system, where it serves to enhance contrast between points of different illumination, as first shown for ganglion cells in the retina (Kuffler 1953) and subsequently at higher levels of visual processing. In the olfactory bulb, a combination of experimental and computational approaches identified a model of interactions between mitral and granule cells which predicted a dendrodendritic synaptic circuit mediating self and lateral inhibition of the mitral cells. This has been useful in guiding and accounting for a variety of experimental results (Rall et al. 1966; Rall and Shepherd 1968; Shepherd and Brayton 1979; Xu et al. 2003; Schoppa et al. 1998; Urban and Sakmann 2002; Egger and Urban 2006).

Yokoi et al. (1995) showed preferential tuning of mitral cells to different members of a homologous chemical series. Sharpening of the tuning by inhibition of neighboring members of the series implied a spatial center-surround organization. It was proposed that lateral inhibition, through the dendrodendritic synapses of mitral cells receiving inputs from different olfactory sensory neuron subsets (Ressler et al. 1994; Vassar et al. 1994; Mombaerts 1996), mediates this odor refinement and contrast enhancement. Previous modeling studies have implemented this contrast phenomenon (e.g. Davison et al. 2003; Cleland and Linster 2005; Linster and Hasselmo 1997).

The original dendrodendritic model accounts for such interactions between nearby mitral cells. However, evidence

from odor maps in the glomerular layer (Xu et al. 2003; Leon and Johnson 2003; Mori et al. 2006) shows that neighboring members of a homologous chemical series activate not only clusters but also widely distributed glomeruli. This activation of widely distributed glomeruli has come to be referred to as "non-topographical", i.e. non-neighboring glomerular, odor representation (Cleland and Sethupathy 2006). Long range connections of up to a millimeter or more are required for lateral inhibition to occur between mitral cells belonging to these distributed glomeruli.

How is the dendrodendritic microcircuit incorporated into this more widely distributed network? We analyze this question with realistic cell properties and network connectivity in order to test the hypothesis that propagating action potentials in mitral cell lateral dendrites play a critical role. We focus on a single respiratory cycle, which has been shown to be sufficient for odor recognition (Uchida and Mainen 2003; see also Abraham et al. 2004). The results provide new insights into the nature of lateral inhibition through active lateral mitral cell dendrites and the columnar organization of granule cells. They predict a new function for granule cells in providing for selective control of activity in individual mitral cell lateral dendrites with minimal effect on soma and other lateral dendrites. The results depend on the dendritic architecture and cannot be obtained with reduced or artificial networks. The model predicts new specific computational roles of granule cells in processing the odor maps for output to the cortex.

2 Methods

All the simulations were carried out with the NEURON simulation program (Hines and Carnevale 1997, v5.8) using its variable time step feature. The model and simulation files are available for public download under the ModelDB section of the Senselab database (http://senselab.med.yale.edu).

2.1 Electrophysiological properties

Mitral cells were implemented as explained in a previous paper (Migliore et al. 2005), with a reduced model including an axon, soma, a primary dendrite, a tuft, and two 500 μm long secondary dendrites. Granule cells (GC) were modeled with a soma, a main radial dendrite (150 μm long) connected to 3 (100 μm long) second order dendrites representing the medial and distal dendritic tree. To test for local effects, three synapses (one in each secondary branch) were explicitly modeled with two additional compartments for spine head and neck. Except where otherwise noted, for all cells we used $R_a = 70$ Ω·cm, and $\tau_m = 30$ ms, with R_m and C_m adjusted to obtain, under control conditions, an

input resistance of about 70 MΩ and 1 GΩ, for mitral (Mori et al. 1981) and granule cells (Schoppa et al. 1998), respectively. Resting potential was set at −65 mV and temperature at 35°C. The same kinetics (from Migliore et al. 2005) were used for Na, KA, and KDR conductances in all cells.

Mitral cells were modeled as regular firing cells (Fig. 1), with Na, KA, and KDR conductances uniformly distributed over the entire dendritic tree (Bischofberger and Jonas 1997; Debarbieux et al. 2003). Odor inputs were modeled using a synchronous activation, in all tuft compartments, of synaptic inputs modeled with a double exponential conductance change (20 and 200 ms raise and decay time, respectively). Following an odor stimulation, APs can initiate in the tuft or in the primary dendrite for moderate to strong odor inputs (Chen et al. 1997, 2002; Debarbieux et al. 2003), and propagate in the secondary dendrites (Xiong and Chen 2002), as shown in the simulations of Fig. 1. Although the fully active propagation of an AP in a mitral cell lateral dendrite has been consistently demonstrated in many experimental works, there can be conditions for which it can be weaker (Christie and Westbrook 2003) or decremental (Margrie et al. 2001). These effects, which have been suggested to depend on the A-type potassium channels, will add an additional mechanism to those that may modulate the AP backpropagation. As discussed later, they will not be explored here.

A peak conductance in the range 0.3–1 nS for each input synapse was used to implement weak or strong odor stimulation. Since our model for the tuft of a mitral cell included 20 branches (Migliore et al. 2005) a total aggregate input conductance of 6–20 nS was used to model each odor input. The total peak conductance on each mitral cell activated by each odor is reported in Table 1.

In granule cells, Na^+ and KA channels were distributed throughout (Schoppa and Westbrook 1999; Zelles et al. 2006; Pinato and Midtgaard 2004) whereas KDR was present only in the soma (Schoppa and Westbrook 1999). In agreement with experimental findings (Schoppa and Westbrook 1999), the dendritic KA resulted in a significant effect on the spike latency of these cells, as shown in Fig. 1(b *b*), and adaptation under strong inputs (Wellis and Kauer 1994; Cang and Isaacson 2003).

2.2 Synaptic and network connections

Effective dendrodendritic coupling between granule cell synapses and mitral cell secondary dendrites was implemented by connecting a GC synapse, containing the same proportion of AMPA and NMDA channels, with each of the three selected compartments of the mitral cells secondary dendrites (see Fig. 1(a)), containing GABA channels. The AMPA conductance was modeled as an alpha-function with

(a) mitral cell properties
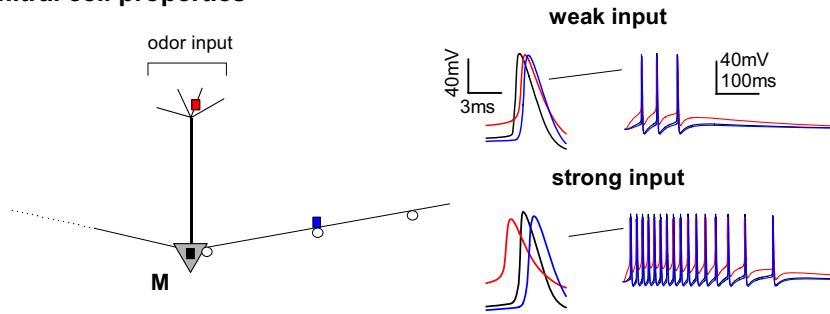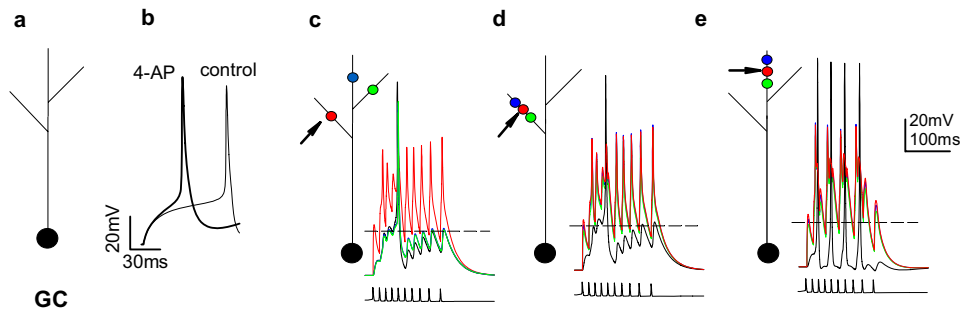

(b) granule cell properties

Fig. 1 Basic properties of the two kind of cells that we used in our model. (**a**) (*left*) Schematic representation of the mitral cell morphology; colored squares indicate recording locations for which membrane potential is shown on the right; open circles indicate locations of the inhibitory synapses from granule cells; (*right*) membrane potential at different locations (lines color correspond to locations indicated on the left part) during a weak (*top*) or strong (*bottom*) odor activation. In both cases, the first action potential is shown on an expanded scale. (**b**) *a* Schematic representation of a granule cell morphology used in the simulations; *b* simulation of the somatic membrane potential during a suprathreshold current step injection under control conditions (*light line*) and after the pharmacological block of the K_A current (*thick line*); *c*, *d*, *e* membrane potential of the soma (*black lines*) and spines (*colored lines*) of a granule cell during a train of mitral cell action potentials (*bottom plots*) activating the red synapse; different synaptic locations were used in *c*, *d*, and *e*; the *dashed lines* represent the threshold for GABA release

a time constant of 3 ms and a reversal potential of 0 mV. The NMDA conductance was based on a NEURON model (Destexhe et al. 1994) of experimental findings (Jahr and Stevens 1990a,b), using an external magnesium concentration of 1 mM and a reversal potential of 0 mV. The model parameters were adjusted to obtain a time-to-peak and decay time constant of 10 and 50 ms, respectively. A double exponential function was used to model the GABA conductance, with a reversal potential of −80 mV. Raise and decay time constants were 1 and 200 ms, respectively, implicitly taking into account all those mechanisms underlying the overall time course observed experimentally

for the inhibitory potential elicited by a single AP in a mitral cell. Unless otherwise noted, the peak excitatory and inhibitory conductance of each synapse were 2.3 nS and 13 nS, respectively. The reversal potential for the inhibitory conductance is higher of the more conventional value of −70 mV expected for GABA_A synapses. Our decision to use a large value was based on experimental data. There are several papers (e.g. Chen et al. 2000; Xiong and Chen 2002; Lowe 2002) showing that the inhibitory potential generated by an AP in a mitral cell can easily hyperpolarize the soma by −15 mV, with respect to rest. However, in the experiments, mitral cells resting potential is somewhat

Table 1 Total peak excitatory synaptic conductance (nS) on each mitral cell activated to model each odor input

Odor	mitra cell 3	4	5	6	7	8	9	10	11
M1	9	13	20	16	8.6	8	0	0	0
M2	0	0	6	11	20	16	7	0	0
M3	0	0	6	9	11	14	20	14	10

variable between −60 and −70. Under these circumstances, to be consistent with the large hyperpolarization observed in many experiments, we have decided to use a larger reversal potential, rather than a higher resting potential. However, test simulations using −70 mV (not shown) demonstrated that the results do not significantly depend on this choice.

Synapses (excitatory or inhibitory) were activated whenever the corresponding presynaptic compartment reached the threshold of −40 mV. In agreement with experimental findings (Isaacson 2001), this choice resulted in recurrent inhibition of the secondary dendrite of a mitral cell that did not necessarily require the generation/propagation of an action potential to the soma of the GC (Fig. 1(b *c–e*)). Furthermore, the relative electrotonic distance between the GC synapses could also determine the amount of lateral inhibition caused by the spread of depolarization to neighbor synapses (Woolf et al. 1991) and the kind of spiking observed at the soma. We tested the effects of different locations for the three synapses explicitly included in our model of a GC, during a train of stimuli generated from a mitral cell (bottom plots in Fig. 1(b *c–e*)) connected to one of the synapse (red circle in Fig. 1(b *c–e*)). In the simulation of Fig. 1(b *c*), the synapses were on electrotonically distant locations. In this case, excitatory input from the mitral cell elicited a train of spikes in the spine (red line) that, however, did not propagate to the other synapses (green and blue lines) or to the soma (black line), where only one spike was observed. Under these conditions, recurrent and lateral inhibition could be drastically different. The time course of the somatic membrane potential did not significantly change when the three synapses were colocalized in the same branch (Fig. 1(b *d*)). This configuration resulted in the same amount of recurrent and lateral inhibition, because the synapses are electrotonically close to each other. The position of the synapses in the dendritic tree can also result in drastically different somatic spiking activity, as shown in the simulation of Fig. 1(b *e*). The different dendritic and somatic spiking patterns originated from both the electrotonic structure of a granule cell and by the relatively long time course of the NMDA conductance. The consequent calcium influx (not included in our model) could thus result in a variety of (somatically subthreshold) local and global calcium transients, consistently with experimental observations (Egger et al. 2003, 2005). Unless otherwise noted, to simplify the illustration of the main results, in all network simulations using 3GCs we positioned the synapses as in Fig. 1(b *d*).

To test the effects of a more detailed network organization into glomerular units, one set of simulations was carried out using groups of 20 GCs, distributed in such a way to allow synaptic connections with the lateral dendrites of the mitral cells at random positions around ±50,

150–250, and 350–450 μm from the soma. Any given GC (configured as in Fig. 1(b *c*)) was connected with each mitral cell by choosing random one synapse and a position along an overlying mitral cell lateral dendrite (within the appropriate region). The peak inhibitory conductance of each synapse was drawn from a normal distribution of 1.2±0.4 nS.

It should be noted that a number of additional mechanisms were not included in our model. Virtually all of them, such as subthreshold oscillations, additional K^+ conductances, persistent Na^+ current, Ca^{2+}-dependent currents, but also activity-dependent changes in channel densities or kinetic, non-uniform distribution of the various Ca^{2+} currents, intracellular Ca^{2+} dynamics, etc, may modulate the process of odor recognition. This is precisely why we did not include them in the model, at this stage. Rather, we were interested in studying dendrodendritic coupling in a realistic network configuration, a process that is quite difficult to study experimentally. For these reasons, we have included only those mechanisms needed for action potential generation and interglomerular synaptic transmission. It would be interesting to include additional cell properties in a future study, to investigate how and to what extent they affect the basic findings shown in this paper.

3 Results

3.1 Distance independent lateral inhibition

It has been shown that lateral inhibition through granule cells is sparse (Urban and Sakmann 2002), suggesting inhibition between sparsely distributed mitral cells. Given that the diameters of glomeruli in the rat are 80–150 μm, mitral cells belonging to different glomeruli are on average likely also to be a similar distance, or multiples thereof, apart. But most granule cell dendritic trees are restricted in extent to approximately the diameter of a glomerulus (Woolf et al. 1991). This means that when mitral cells are far apart their interactions are limited, because, as indicated by comparing Fig. 2(a) and (b), the effect of the inhibition weakens with distance along the lateral dendrite because of electrotonic attenuation. A model with a simple center-surround organization between neighboring cells cannot thus easily account for these interactions. By contrast, we hypothesized that mitral cell lateral inhibition can be optimal if it is exerted through an action potential fully propagating along a mitral cell lateral dendrite (Fig. 2(c)), as demonstrated experimentally (Xiong and Chen 2002).

A second hypothesis has related to the nature of the organization of the granule cells. This builds on a recent study (Willhite et al. 2006) involving viral tracing of connectivity in the olfactory bulb. Virus transported
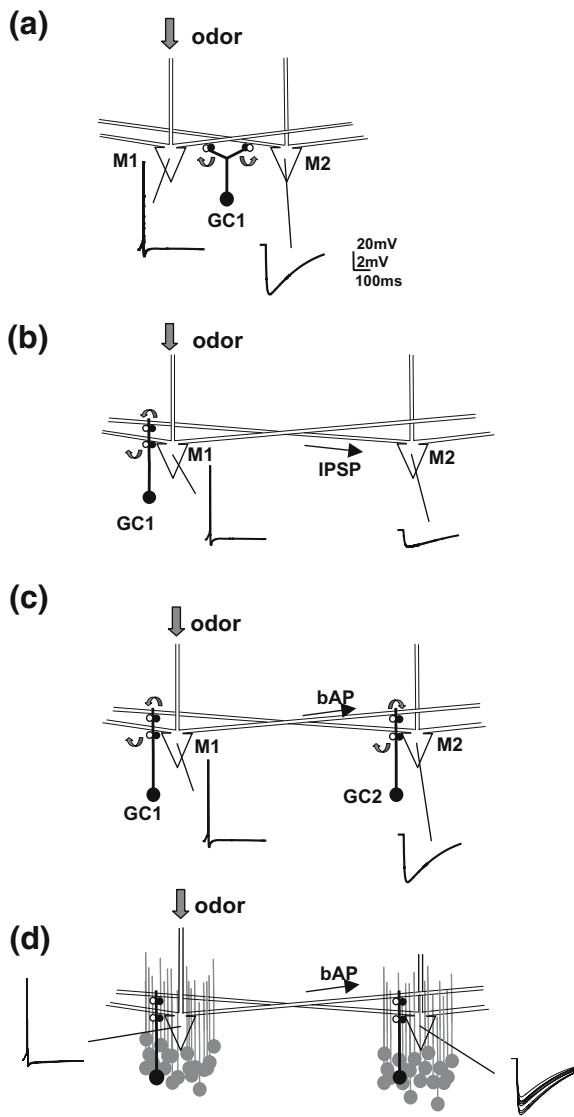
Fig. 2 Non-topographical connectivity of the granule–mitral cells network requires a new paradigm for an efficient lateral inhibition mechanism; traces are mitral cell model (*M1-2*) somatic recordings; dendrodendritic synapses between mitral and granule cell (*GC1-2*) indicated with curved arrows and open (excitatory) and closed (inhibitory) circles. (**a**) Original model of spatial center-surround organization of lateral inhibition in the olfactory bulb. (**b**) Increasing the distance between mitral cells (belonging to different glomeruli) weakens the inhibition of the distant cell: the inhibitory postsynaptic signal (*IPSP*) spreads decrementally in the lateral *M2* dendrite to reach the soma. (**c**) Inhibition can be independent of distance if it is imposed locally by granule cells activated by a backpropagating action potential (*bAP*). (**d**) Schematic representation of the larger network used to test action potential-mediated lateral inhibition in a more realistic arrangement for a glomerular unit; groups of 20 GCs were clustered around each mitral cell soma, forming random dendrodendritic contacts with overlaying lateral dendrites. Traces are mitral cell somatic recordings from 10 simulations; for clarity, only one granule cell and its connectivity (*open* and *closed circles*) are explicitly drawn

through the mitral lateral dendrites has shown labelled mitral and granule cells grouped in a column, and further that a column is related to a glomerulus, thus forming a "glomerular unit". In addition, multiple columns labelled from a single injection site are widely distributed in the olfactory bulb, indicating that such distributed glomerular units are likely involved in processing of similar information contained in the equally widely distributed odor maps (Leon and Johnson 2003; Xu et al. 2003). Since the mitral cell lateral dendrites extend for up to 1 mm in length, they provide an effective way of activating granule cells connected to glomerular units at variable "non-topographic" distances from an activated mitral cell. The combined model shown in Fig. 2(c) is thus strongly supported by experimental evidence.

It may be questioned if this effect, obtained with a reduced network and a single relatively large inhibitory synapse (modeling the cumulative effect of about 20 electrotonically close real inhibitory inputs), can be also obtained with a larger network of GCs distributed over a region that could be as wide as a glomerulus diameter. We then randomly clustered 20 GCs around ±50 μm from the soma of each mitral cell, randomly connecting their synapses (1.2±0.4 nS, corresponding to about two individual synapses) with an overlying lateral dendrite, as schematically shown in Fig. 2(d) (see the "Methods" section). In reality, the granule to mitral connections are laid down during development, presumably by a learning process underlying the connectivity between mutually activated glomerular units. The two mitral cell somata were 400 μm apart. Using 10 different random distributions of GCs synapses on mitral cell dendritic locations and the same stimulation protocol (a mitral cell input eliciting a single AP), we consistently obtained a large inhibitory effect (traces on the right in Fig. 2(d)), confirming the results obtained with the reduced three GCs network (compare M2 traces in Fig. 2(d) and (c)). It should be stressed that there are about 25 mitral cell belonging to the same glomerular unit, and there are up to 100 GCs per mitral cell (Shepherd and Greer 1998). This means that each mitral cell could receive up to approximately 2,500 different inhibitory inputs (one from each GC) clustered in the proximal region of its lateral dendrites. Assuming an average value of 0.6 nS per synapse (Schoppa et al. 1998), our simulations reveal that only a very small fraction (about 40 synapses in our case) would be needed for an effective lateral inhibition.

To further test our hypotheses, we implemented the network shown in Fig. 3. It was composed of three mitral cells (*M1-3*) and three granule cells (*GC1-3*), fully connected and arranged as schematically represented in Fig. 3. Mitral cells were assumed to belong to different glomerular units. Each granule cell formed dendrodendritic
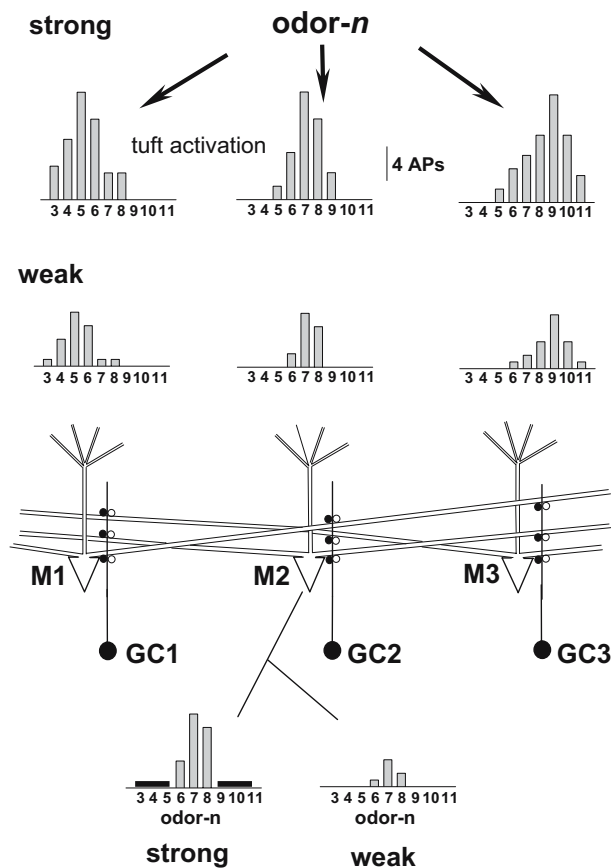
Fig. 3 Schematic representation of the reduced network used in most simulations, and its effect for different odor inputs ($n=3\dots11$). M1, M2, and M3 indicate Mitral cells, GC1, GC2, and GC3 indicate granule cells. Uniform all-to-all connectivity was assumed in this case. Each histogram represents the number of somatic APs elicited in a given mitral cell by each odor input without (*top histograms*) or in the presence of granule cells in the network (*bottom histograms*). The effect of lateral inhibition in abolishing M2 output for flanking odors is schematically represented by the black bars; *Weak* input was modeled with a 60% reduction of the *strong* one. Locations of dendrodendritic synaptic contacts are indicated with small *open* and *closed circles*. In all cases, synapses on the granule cells were positioned as in Fig. 1(b *d*); for clarity, each GC is represented with only the branch including the synapses

synapses with one of the secondary dendrites of each mitral cell, at a location determined by the geometrical network arrangement. In our case, mitral cells were assumed to be about 200 μm apart. This resulted, for example, in *GC1* forming dendrodendritic synapses close to the soma of *M1*, at about 200 μm with *M2*, and at about 400 μm from the soma with *M3*.

We reanalyzed the odor refinement effect caused by lateral inhibition of mitral cells by granule cells using this new network architecture. It was experimentally shown (Yokoi et al. 1995) that a mitral cell response to molecularly similar odor molecules shows a strong response to a

"preferred" molecule, and decreasing activity for similar but distinct odor molecules, with different mitral cells showing preference for different molecules in a series. We implemented the responses of three model mitral cells to a set of nine odors by adjusting the input peak conductance in such a way to reproduce approximately the experimental findings (Yokoi et al. 1995). In Fig. 3 the top histograms represent the number of APs generated by each odor in each mitral cell in the absence of the GCs; as expected, they reflect the spectrum of the input, with stronger inputs eliciting more APs (Table 1). Two sets of input were used (Fig. 3, strong and weak). For the purposes of the present paper, we define the contrast, c, between the output of M2 and Mx ($x=1$ and 3) as $c=(1-s2/sx)$, where $s2$ and sx are the number of spikes elicited in M2 and Mx, respectively.

By comparing the output of M2 for the non-preferred odor-5 (preferred by M1) and odor-9 (preferred by M3) with or without the GCs (Fig. 3, top and bottom histograms, respectively) one can clearly see the effect of the GCs: 16 spikes were elicited in M1 and M3 by odor-5 and -9, respectively, whereas only two and three spikes were elicited in M2 without GCs. This corresponded to a contrast of 87.5% and 81%. However, they were completely abolished in the presence of GCs: a 100% contrast, even if the feedforward inhibition reduced to 11 spikes the output of M1 and M3 to odor-5 and -9 (data not shown). This is the basic mechanism of contrast enhancement between the inputs to M2 and its neighbors. This was a robust finding in our simulations, and is closely similar to the experimental results and the model proposed by Yokoi et al (1995). It is consistent with the current view on the implementation of odor contrast through lateral inhibition, and can be considered as a control condition of our network operation. Note that this network arrangement is able to implement strong lateral inhibition between mitral cells belonging to different glomerular units at arbitrary distances, limited only by the extent of action potential propagation along the mitral cell secondary dendrites.

An experiment demonstrating a specific example of the effect in Fig. 3 is shown in Fig. 4, with recordings of the responses of a single cell to three different, but closely related, odors during a single respiratory cycle. In this control condition the tuning is very sharp for only hexylaldehyde, with essentially no response to odor molecules differing by only two carbon atoms longer or shorter.

We wished to carry out a more detailed analysis of the mechanism of the proposed inhibitory circuit underlying this effect. In the model of the somatic recordings of M2 to correspondingly graded odor inputs as shown by the histograms in Fig. 3, the responses are similarly sharply tuned (Fig. 4(a), right): the model cell responds briskly to odor 7 and is inhibited by odors 5 and 9. The inhibition is
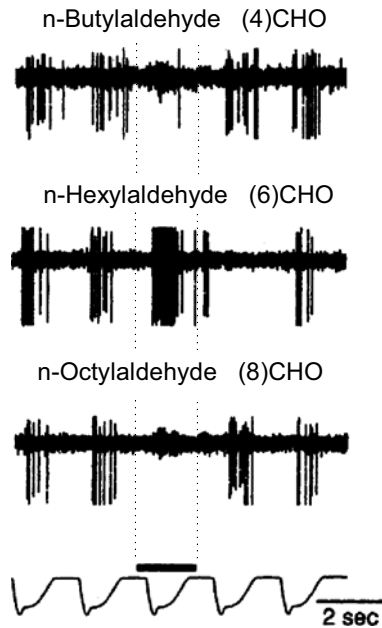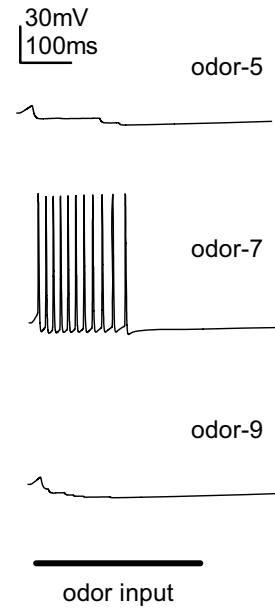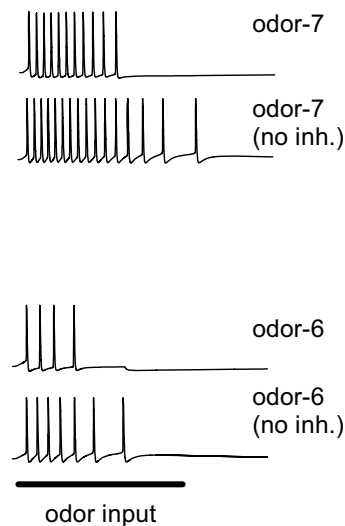
Fig. 4 Effects of lateral inhibition and comparison with experiments. (**a**) (*left*) Single unit recordings of mitral cells activity during presentation of different odors (4-, 6-, and 8-CHO); (*right*) somatic potential of a mitral cell from our model (*M2*) during presentation of different odors (5, 7, and 9); (**b**) (*left*) experiments, effects of bicuculline application; (*right*) model, somatic membrane potential of *M2* during odor presentation after block of dendrodendritic interactions. Experimental traces taken and redrawn from Yokoi et al. (1995)

due to the preferential activation of other mitral cells to odors 5 and 9 (equivalent to butylaldehyde and octylaldehyde in the experiments). Note that the IPSPs in the recorded mitral cell in response to these two odors are not symmetrical; this is because of the differing molecular receptive ranges (MRRs) of the flanking MCs. The model therefore predicts that comparisons of IPSPs can reflect different MRRs of other MCs. When inhibition was blocked in the experiments by bicuculline, the firing activity increased for both weak and strong inputs. This effect was also reproduced by the model in Fig. 4(b).

3.2 Detailed analysis of APs backpropagation in a lateral dendrite

Further analysis of the model gave insights into the interplay of the mechanisms involved in the operation of this small circuit. For this purpose, preferential input was directed to a lateral member of the three mitral cell circuits, so that events taking place within the elongated lateral dendrites extending across two glomerular units could be investigated. This is illustrated in the simulation of Fig. 5, where we track many model variables during the first 300 ms of an odor presentation (i.e. "sniff"). For this example we use odor-9, which, as shown in Fig. 3, gives strong excitation of M3, weak of M2, and no activation of M1. The model "experiment" starts with "odor" activation of the excitatory input conductances on the mitral cell tufts. Each mitral cell receives a different amount of excitation (Fig. 5, input) reflecting the odor molecular receptive range in Fig. 3 as described above.

The prolonged time course of the EPSPs is shown in Fig. 5(a). They activate the action potential response in M3, the cell receiving the strongest input. This strong input gives rise to a forward propagating action potential in the primary dendrite, as shown experimentally (Chen et al. 1997), with backpropagation into the secondary dendrites (Xiong and Chen 2002; Lowe 2002). Our model revealed the complex effects that take place in the secondary dendrites during the invasion of successive action potentials.

We focus particularly on the initial two spikes in response to these EPSPs in the mitral tuft. The first spike in the M3 lateral dendrite leads to an IPSP in the proximal M2 lateral dendrite that spreads to the nearby cell body (see red trace in Fig. 5(b)). The EPSP in the granule cell GC1, however, does not reach threshold for GABA release on M1 (shown in black trace; see discussion of Fig. 5(d) below). However, the second spike in M3 leads to inhibition of both M1 and M2 because the corresponding granule cells reach threshold for GABA release in both cases (see discussion of Fig. 5(d) below).

In accord with physiological evidence (Xiong and Chen 2002; Lowe 2002), the spike propagates through the secondary dendrites with very little delay (Fig. 5(c), M3 secondary dendrite). Note that the first three action potentials in the dendrites are progressively reduced in amplitude, due to the buildup of the successive IPSPs through the dendrodendritic synapses. Interestingly, the middle site shows the most reduction, due to the greater conductance load, compared with the distal site, which has the advantage of the terminal boundary condition (sealed end effect).

The site of AP failure will of course reflect multiple factors, especially the distribution of the granule cell inhibitory inputs. In our model the first to fail is the middle site, where there is reduction to a small spike due to the electrotonic spread from the full spike in the soma and proximal portion of the dendrite (small fourth red spike in Fig. 5(c)). This small spike in turn spreads electrotonically to the distal site to give a small transient (small fourth black spikelet in Fig. 5(c)). The middle amplitude spikes sometimes reach threshold for GLU release and consequent dendrodendritic feedback, but the small spikelets are always below threshold (see dashed line).

While all this activity, including strong inhibition of spike backpropagation, is occurring in this lateral dendrite, the soma continues to generate full amplitude action potentials at a relatively steady firing frequency (compare with B). This means, in addition, that other lateral dendrites arising from the same mitral soma are relatively unaffected by the activity in a given lateral dendrite.

These events in the lateral dendrite are direct consequences of the dendrodendritic interactions with the three GCs. As already indicated, it is essential to compare these events in the mitral cells with those in the granule cells, as shown in Fig. 5(d), GC1-3. Although all the recurrent contacts activate inhibitory currents on M3 (as shown by the curves from GC1-3), lateral inhibition was activated on M2 (Fig. 5(b), red line, hyperpolarization just after the first spike on M3) but not in M1 (Fig. 5, black line, no hyperpolarization after first M3 AP). The second AP on M3 generates lateral inhibition on both M1 and M2 (Fig. 5, note M1 and M2 hyperpolarization after the second M3 spike). A somatic AP in the GCs is elicited only after the third M3 spike. After these three M3 spikes, the buildup of a powerful inhibitory conductance on the secondary dendrite of M3 shunts the backpropagation of additional APs. Most of the following somatic APs of M3 are strongly reduced in their amplitude beyond approximately 200 μm from the soma. Most of them will fail to cross the threshold for GLU release, effectively reducing or terminating the local dendrodendritic interaction with the GC cells (Fig. 5,

Fig. 5 Detailed dynamics of the interaction between mitral and granule cells during an odor presentation, using the network in Fig. 3. (**a**) Time course of the input excitatory conductance, corresponding to odor 9, activated in the tuft of each mitral cell (M1, M2, M3); for the purpose of this figure, the total peak excitatory input on M3 and all the peak inhibitory conductances were 17 and 18 nS, respectively. (**b**) Somatic membrane potential of the three mitral cells during odor presentation. (**c**) Membrane potential of one of the secondary dendrites of mitral cell M3 at different distances from the soma; the *dotted line* indicates the threshold for the activation of the mitral-to-granule excitatory synapse. (**d**) Membrane potential of the granule cells at the location of the dendrodendritic synapse with mitral cell M3 (*top plot*) and at the soma (*bottom plot*) during odor presentation. (**e**) Time course of the local dendritic inhibitory conductances activated on the M3 secondary dendrite during odor presentation
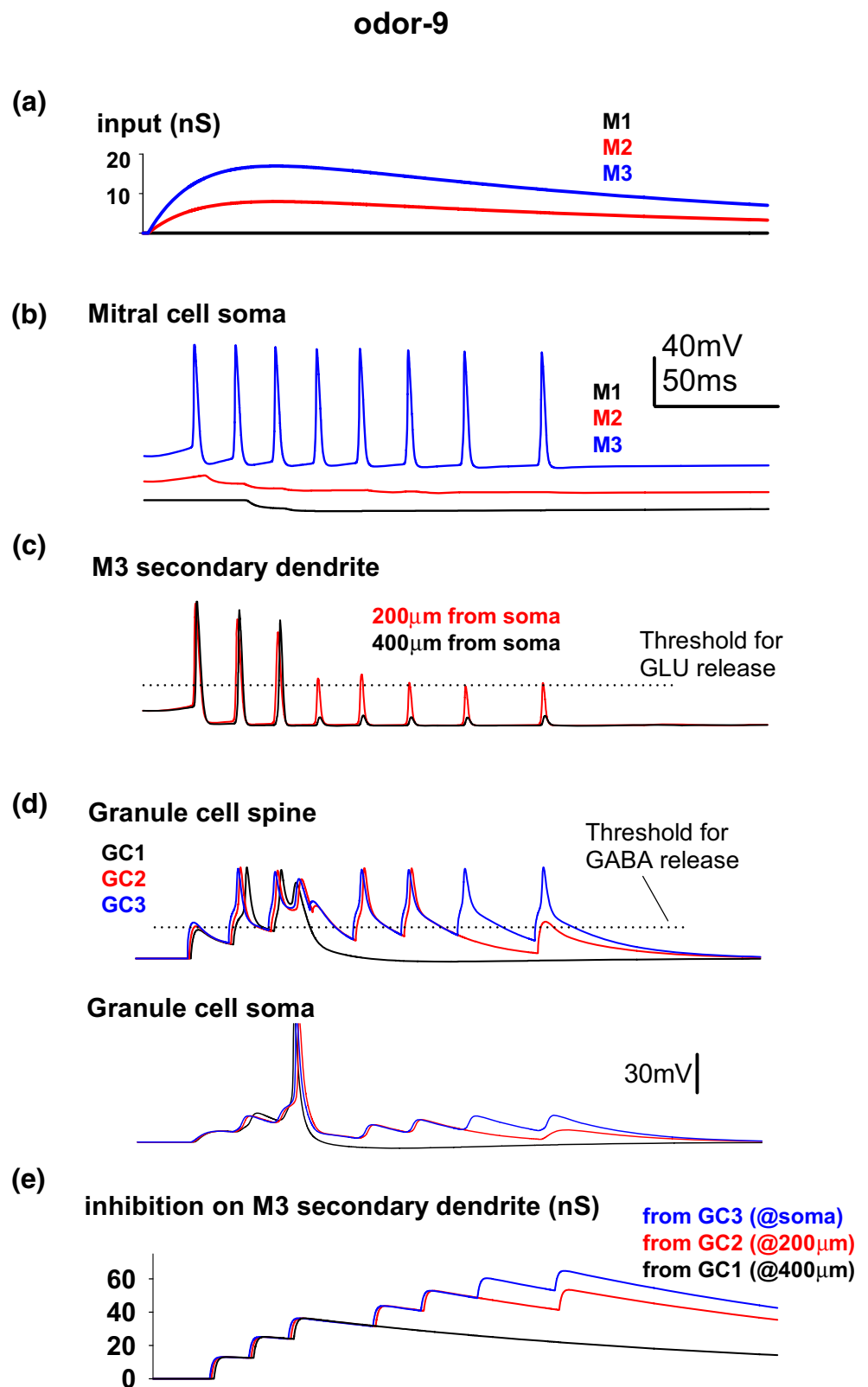
inhibition on M3, compare black, red and blue lines after the third M3 spike). It should be stressed that this effect could be limited to the mid and distal portion of the secondary dendrite, and occurs in the presence of a train of somatic M3 spikes that does not show any sign of strong amplitude reduction or missing spikes (Fig. 5(b–c), compare M3 soma with M3 secondary dendrite).

The explicit inclusion in the model of lateral dendrites directly interacting with granule cells, and the consequent conditional AP backpropagation, may affect the network operation in unpredictable ways, in comparison with a network composed only of simpler elements. To highlight the possible differences, we modified our network to obtain the same all-to-all connectivity through mitral cell somata rather than lateral dendrites, as schematically represented in Fig. 6, using the same odor inputs as in Fig. 3. The crucial

point was the direct connection between each granule cell and the soma of each mitral cell. Although, with an appropriate scaling of the peak inhibitory conductances (from 13 to 9 nS), the results from the point of view of contrast enhancement for M2 were similar to those obtained before (100% for odor-5 and -9, compare M2 output with that in Fig. 3, strong input), the granule cell dendritic membrane potential was rather different (compare GC1 and GC2 traces in Fig. 6 with Fig. 5(d)). In fact, all the granule cells received, by construction, the same input (only from M2, in this case). This means that during a train of mitral cell spikes they will deliver an inhibitory signal every AP (until saturation), greatly increasing both the feedforward and lateral inhibition. This findings suggest that during presentation of odors with more complex activation patterns, the output of a set of such mitral cells might be
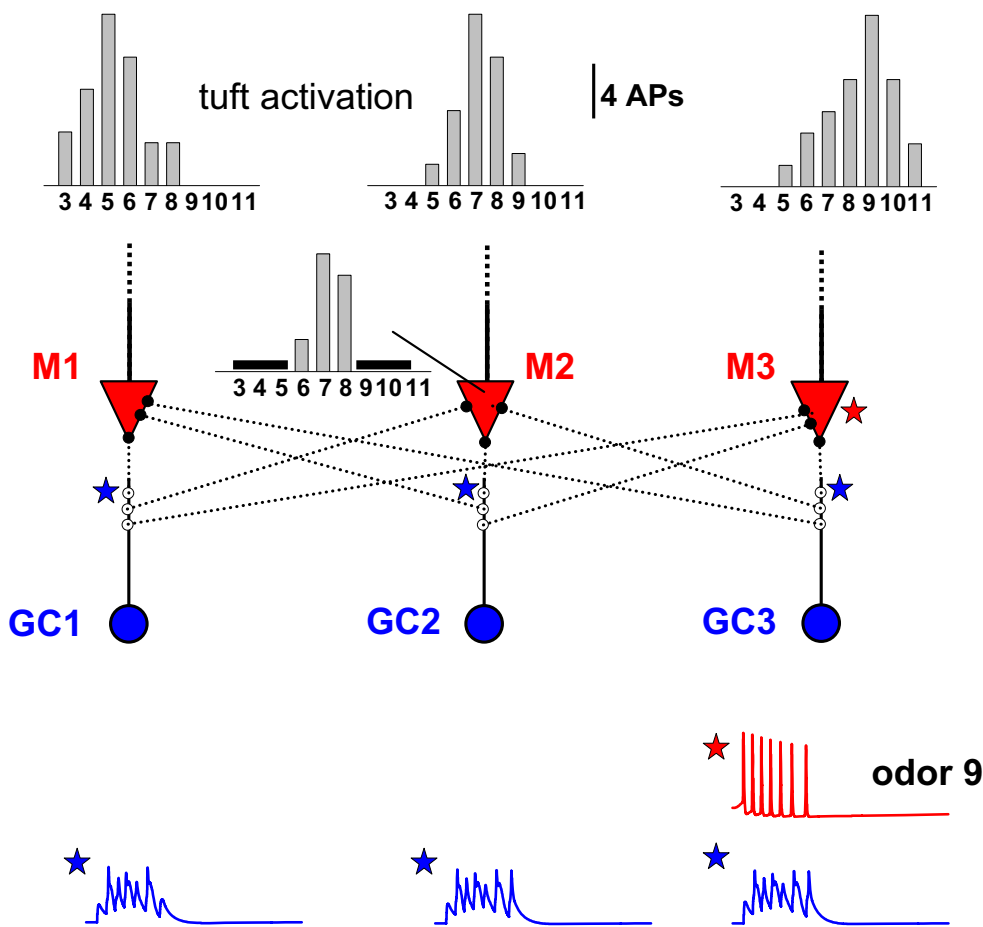

Fig. 6 Schematic representation of a network using mitral cells without lateral dendrites, to test the effect of different odor inputs as in Fig. 3. M1, M2, and M3 indicate mitral cells, GC1, GC2, and GC3 indicate granule cells. Uniform all-to-all connectivity was arranged through mitral cells soma and granule cell dendrites; Top histograms represents the number of somatic APs elicited in a given mitral cell by each odor input without granule cells in the network. The response of M1 in the presence of the granule cells network is reported in the bottom histogram. *Weak* input was modeled with a 60% reduction of the *strong* one. Locations of dendrodendritic synaptic contacts are indicated with small open and closed circles. In all cases, synapses on the granule cells were positioned as in Fig. 1(b *d*), with a peak inhibitory conductance of 9 nS; traces were obtained from a simulation with a total synaptic input on M3 of 17 nS, as in Fig. 5

Fig. 7 Model of predicted gating effects during odor presentation. Arrow thickness represents the strength of the input to each mitral cell tuft, and locations of dendrodendritic synaptic contacts are indicated with small *open* and *closed circles*. (**a**) Traces are shown at selected locations (*colored squares*) and shown in different colors; (*red*) mitral cell soma, (*blue*) granule cell soma, (*cyan*) granule cell synapse with M2 lateral dendrite, (*orange*) M1 lateral dendrite at 200 and 400 μm from the soma; note that the odor does not activate M2. (**b**) As in (**a**) but with an odor that also activates M2. Note the EPSPs in GC2, activated by M2 (*cyan*). The spike train of M1 (*orange*) decrements because local synaptic activity in GC2 (*cyan*). Experimental traces (*exp*) from Lowe (2002)

(a) inhibitory effect of M1 on M3

odor-a

40mV
100ms
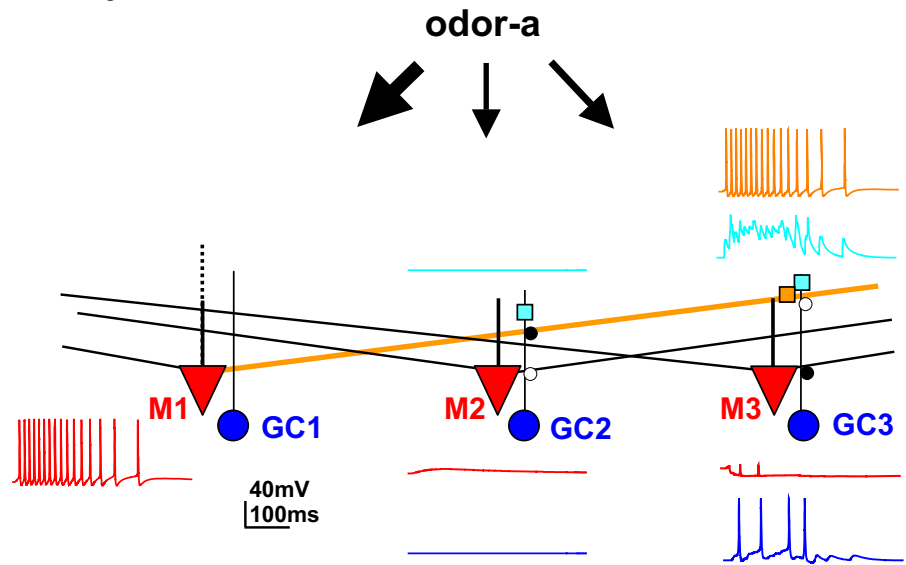
(b) M2 gates inhibitory effect of M1

odor-b

exp

soma   93μm
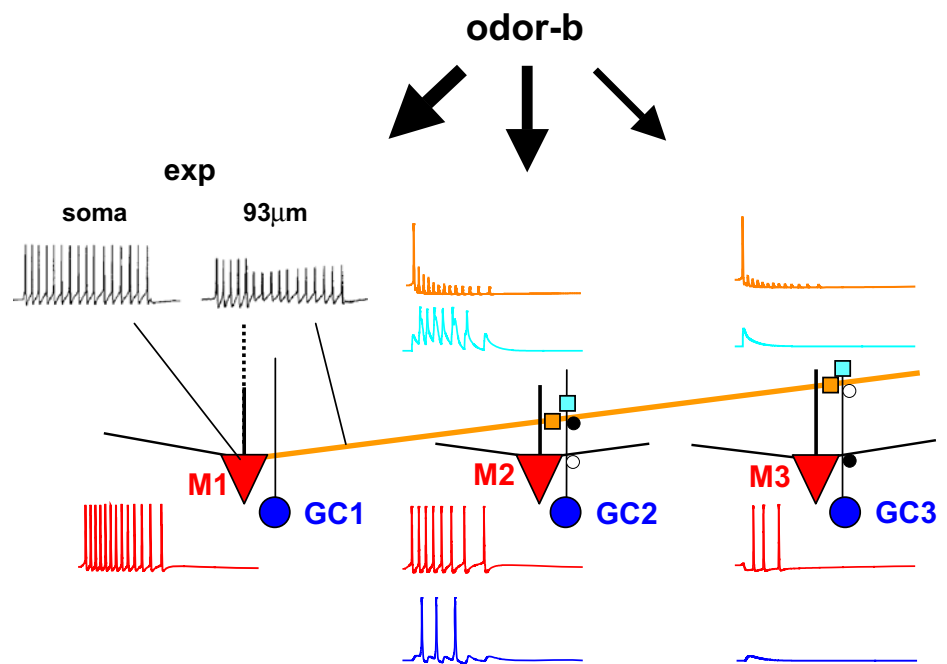
considerable different from that obtained with a more realistic implementation with lateral dendrites.

3.3 Functional consequences of APs backpropagation blockage

A significant effect seen in the lateral dendrites is the blockage of AP backpropagation after several initial full spikes, which has been documented experimentally (Lowe 2002). Furthermore, the extensive action potential propagation in the lateral dendrites opens up new possibilities of local modulation of the action potentials to affect network operations. To illustrate one of these cases, we used a network with minimal connectivity as illustrated in Fig. 7: there are only two sets of excitatory and inhibitory synapses, connecting M2 and M3 with one of the lateral

dendrites of M1. A fourfold increase in the peak inhibitory conductance was used in this case, corresponding to activate approximately 85 different synapses, well below (approximately 4%) of those that could be theoretically available within a glomerular unit. In Fig. 7(a), an odor

(odor-a) activates the dendritic tufts of M1, M2 and M3 with different strengths, represented by arrows of different sizes: M1 receives a strong input, M2 a weak subthreshold input, and M3 a moderate input. Under these conditions, lateral inhibition generated by the dendrodendritic coupling
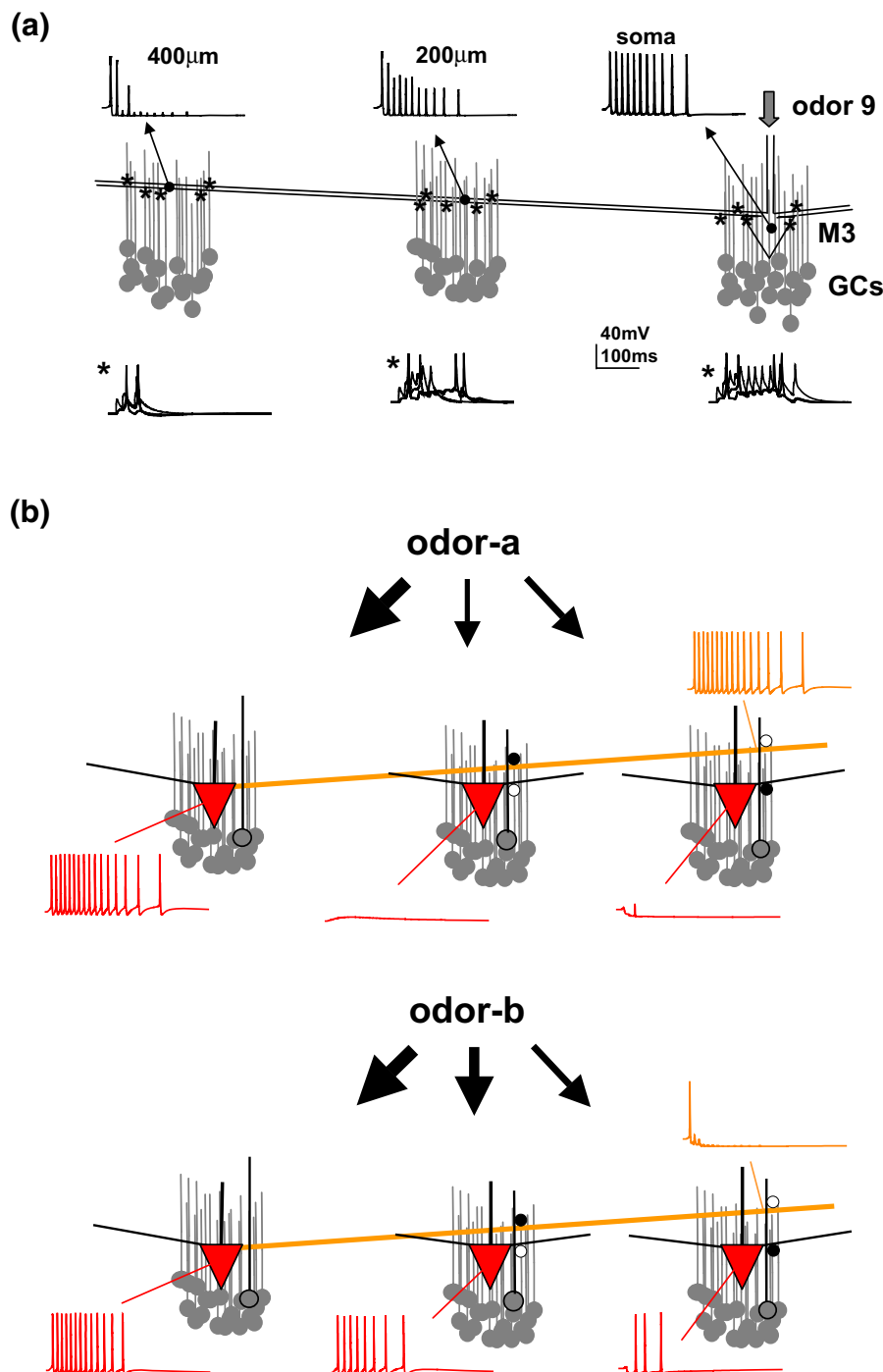

Fig. 8 Gating of action potential backpropagation with a larger GC network. (**a**) Typical traces from a simulation during presentation of odor-9; (*top*) membrane potential of M2 at the soma and lateral dendrite at 200 and 400 μm from the soma; (*bottom*) overlapped dendritic recordings from five GCs. (**b**) Somatic and dendritic recordings during presentation of odors *a* and *b* as in Fig. 6; (*red*) mitral cells soma; (*orange*) M1 lateral dendrite at 400 μm from the soma; compared with the analogous traces in Fig. 6

between the propagating action potentials of M1 (Fig. 7, orange trace) and the corresponding synapse with GC3 (Fig. 7, cyan trace) results in a strong inhibitory effect on M3, which prevents M3 from spiking. However, if M2 receives a stronger, suprathreshold, input (as in Fig. 7(b), odor-b) M2 fires, strongly activating GC2.

If a granule cell such as GC2 has synapses through its radial extent with lateral dendrites passing through from other mitral cells such as M1, the model shows that the connectivity will have interesting gating effects. The first propagating action potential into the M1 lateral dendrite will be successful, but the coupling between M1 and GC2 will shunt subsequent M1 backpropagation to GC3 (Fig. 7, orange trace at GC3). This strongly reduces the activation of GC3 and thus M3 inhibition. The strength of activation of M2 thus can determine gating of the lateral inhibition from M1 on M3. The shunting mechanism of back-propagating action potentials has been observed experimentally with focal application of GABA (Xiong and Chen 2002; Lowe 2002). This kind of veto over long distance signal propagation might have far reaching consequences for the binding process needed for odor recognition, and will be discussed in more detail in a future paper.

3.4 Results using a larger GCs network

To test the robustness of our model, we finally tested if the major findings obtained with the reduced 3GCs model, i.e. the modulation of AP backpropagation (Fig. 5) and gating of functional connectivity (Fig. 7), can be obtained with a larger and more distributed GC network. Three groups of 20GCs were randomly positioned around the soma of each mitral cell according to the same algorithm used in for Fig. 2(d) (see Methods), as schematically shown in Fig. 8. To test for modulation of AP backpropagation, we stimulated only M3 using odor 9 as in Fig. 5. Typical recordings for M3 soma and lateral dendrite are shown in Fig. 8(a). The simulation confirmed the results of the reduced network: most of the APs during a train failed to reach the distal region of the lateral dendrite (Fig. 8(a), trace at 400 μm), because of the lateral inhibition elicited by the three columns of GCc. Dendritic recordings from five randomly chosen GCs are shown in Fig. 8(a) (bottom), and demonstrate the different firing patterns generated in each GC, resulting from a different position and/or connectivity within the column. The gating effect was tested by using the same inputs (odors a and b) and minimal connectivity as in Fig. 7. In this case, the peak conductance for the two sets of inhibitory synapses on M1 and M2 (see closed circle in Fig. 8(b)) were increased 12- and 6-fold, respectively. This would correspond to activating approximately 250–500 different synapses, again well below (approximately 10–20%) the maximum available

theoretically. Typical traces from a simulation (Fig. 8(b)) gave results nearly identical to those obtained with three GCs (Fig. 7), demonstrating also in this case the robustness of the model's prediction.

4 Discussion

The results give several new insights into the mechanism of lateral inhibition in the olfactory bulb and its possible significance for odor processing. Some of these points have been noted in the Results, and we summarize the salient ones here.

4.1 Lateral inhibition through granule cells

The results show that GCs can give contrast enhancement between differentially activated glomerular units, as reported experimentally (e.g. Yokoi et al. 1995) and computationally (e.g. Davison et al. 2003) by many authors (reviewed in Cleland and Linster 2005). They are also consistent with the emerging concept that lateral inhibition is directed toward glomerular units processing information about structurally related odor molecules.

Our model introduces the new notion that backpropagating action potentials in the long lateral dendrites of mitral cells, together with granule cell actions on mitral cells within narrow columns forming glomerular units, can provide the means to activate strong local inhibition between arbitrarily distant mitral cells. Full action potential backpropagation through the lateral dendrites of mitral cells is thus the mechanism for obtaining activation of granule cells independent of distance. This new paradigm fits with recent experimental studies, and allows a functional wiring of the olfactory bulb that could greatly expand the computational roles of the mitral–granule cell network. The model also indicates a new level of specificity, in that individual lateral dendrites act as semi-independent sources of the signals for the lateral interactions. This is further evidence against the idea of a smooth spatial surround around an activated glomerulus, in favor of discrete targeting of lateral inhibition in a given lateral dendrite with its specific relation to overlying glomeruli (Willhite et al. 2006).

4.2 New implications for the mechanism
    of dendrodendritic inhibition

We have hypothesized a new function for dendrodendritic inhibition, as having its main effect in gating action potential backpropagation in individual lateral dendrites, in order to modulate odor processing in a selective manner through surrounding olfactory glomerular units. The

exploration of the functional consequences of this local effect for odor processing requires further (experimental and modeling) study. The relative strength of the two functions of dendrodendritic inhibition will depend on the strength of the IPSPs and on the divergence of connectivity of the granule cells. The emerging picture is one in which the MCs collect the glomerular outputs and distribute them through the olfactory bulb by means of action potentials independently propagating through their lateral dendrites. The GCs modulate the spread of the signals through their selective inhibitory action on the lateral dendrites. This action creates a context-dependent ensemble of activity that constitutes the output to the olfactory cortex.

4.3 Critical importance of dendritic architecture and connectivity

As a general comment, we note that the realistic architecture used in these simulations has been essential for bringing out new features of the network mechanisms that may be involved in odor processing. We have shown that specific properties, such as the possibility to modulate AP propagation between glomerular units, likely to be critical in odor processing (Egger and Urban 2006), requires specific features such as long lateral dendrites of mitral cells and specific connectivity of granule cells arranged in columnar populations.

It should be stressed that this mechanism for AP gating can operate in the presence of a train of full amplitude spikes at the soma and other lateral dendrites. The model predicts that it occurs because of the relatively long electrotonic length of the lateral dendrite. Furthermore, this kind of operation cannot be represented by modeling the network elements with single nodes or nodes with dendrites which lack realistic cable or active properties. In such single node models, firing at the somas is by default the same as occurs in the dendrites, without the relative independence from the local compartmentalization of the inhibition that occurs in the lateral dendrites in the realistic case. It is an example of the computational limitation forced on a nonrealistic network by an oversimplified architecture (cf. Migliore et al. 2005).

References

Abraham, N. M., Spors, H., Carleton, A., Margrie, T. W., Kuner, T., & Schaefer, A. T. (2004). Maintaining accuracy at the expense of speed: Stimulus similarity defines odor discrimination time in mice. *Neuron, 44*, 865–876.

Bischofberger, J., & Jonas, P. (1997). Action potential propagation into the presynaptic dendrites of rat mitral cells. *Journal of Physiology, 504*, 359–365.

Cang, J., & Isaacson, J. S. (2003). *In vivo* whole-cell recording of odor-evoked synaptic transmission in the rat olfactory bulb. *Journal of Neuroscience, 23*, 4108–4116.

Chen, W. R., Midtgaard, J., & Shepherd, G. M. (1997). Forward and backward propagation of dendritic impulses and their synaptic control in mitral cells. *Science, 278*, 463–467.

Chen, W. R., Shen, G. Y., Shepherd, G. M., Hines, M. L., & Midtgaard, J. (2002). Multiple modes of action potential initiation and propagation in mitral cell primary dendrite. *Journal of Neurophysiology, 88*, 2755–2764.

Chen, W. R., Xiong, W., & Shepherd, G. M. (2000). Analysis of relations between NMDA receptors and GABA release at olfactory bulb reciprocal synapses. *Neuron, 25*, 625–633.

Christie, J. M., & Westbrook, G. L. (2003). Regulation of back-propagating action potentials in mitral cell lateral dendrites by A-type potassium currents. *Journal of Neurophysiology, 89*, 2466–2472.

Cleland, T. A., & Linster, C. (2005). Computation in the olfactory system. *Chemical Senses, 30*, 801–813.

Cleland, T. A., & Sethupathy, P. (2006). Non-topographical contrast enhancement in the olfactory bulb. *BMC Neuroscience, 7*, 7.

Davison, A. P., Feng, J., & Brown, D. (2003). Dendrodendritic inhibition and simulated odor responses in a detailed olfactory bulb network model. *Journal of Neurophysiology, 90*, 1921–1935.

Debarbieux, F., Audinat, E., & Charpak, S. (2003). Action potential propagation in dendrites of rat mitral cells *in vivo*. *Journal of Neuroscience, 23*, 5553–5560.

Destexhe, A., Mainen, Z. F., & Sejnowski, T. J. (1994). An efficient method for computing synaptic conductances based on a kinetic model of receptor binding. *Neural Computation, 6*, 10–14.

Egger, V., Svoboda, K., & Mainen, Z. F. (2003). Mechanisms of lateral inhibition in the olfactory bulb: Efficiency and modulation of spike-evoked calcium influx into granule cells. *Journal of Neuroscience, 23*, 7551–7558.

Egger, V., Svoboda, K., & Mainen, Z. F. (2005). Dendrodendritic synaptic signals in olfactory bulb granule cells: Local spine boost and global low-threshold spike. *Journal of Neuroscience, 25*, 3521–3530.

Egger, V., & Urban, N. N. (2006). Dynamic connectivity in the mitral cell–granule cell microcircuit. *Seminars in Cell & Developmental Biology, 17*, 424–432.

Hines, M., & Carnevale, T. (1997). The NEURON simulation environment. *Neural Computation, 9*, 178–1209.

Isaacson, J. S. (2001). Mechanisms governing dendritic gamma-aminobutyric acid (GABA) release in the rat olfactory bulb. *Proceedings of the National Academy of Sciences of the United States of America, 98*, 337–342.

Jahr, C. E., & Stevens, C. F. (1990a). A quantitative description of NMDA receptor-channel kinetic behavior. *Journal of Neuroscience, 10*, 1830–1837.

Jahr, C. E., & Stevens, C. F. (1990b). Voltage dependence of NMDA-activated macroscopic conductances predicted by single-channel kinetics. *Journal of Neuroscience, 10*, 3178–3182.

Kuffler, S. W. (1953). Discharge patterns and functional organization of mammalian retina. *Journal of Neurophysiology, 16*, 37–68.

Leon, M., & Johnson, B. A. (2003). Olfactory coding in the mammalian olfactory bulb. *Brain Research Review, 42*, 23–32.

Linster, C., & Hasselmo, M. (1997). Modulation of inhibition in a model of olfactory bulb reduces overlap in the neural representation of olfactory stimuli. *Behavioural Brain Research, 84*, 117–127.

Lowe, G. (2002). Inhibition of backpropagating action potentials in mitral cell secondary dendrites. *Journal of Neurophysiology, 88*, 64–85.

Margrie, T. W., Sakmann, B., & Urban, N. N. (2001). Action potential propagation in mitral cell lateral dendrites is decremental and controls recurrent and lateral inhibition in the mammalian olfactory bulb. *Proceedings of the National Academy of Sciences of the United States of America, 98*, 319–324.

Migliore, M., Hines, M. L., & Shepherd, G. M. (2005). The role of distal dendritic gap junctions in synchronization of mitral cell axonal output. *Journal of Computational Neuroscience, 18*, 151–161.

Mori, K., Nowycky, M. C., & Shepherd, G. M. (1981). Electrophysiological analysis of mitral cells in the isolated turtle olfactory bulb. *Journal of Physiology, 314*, 281–294.

Mori, K., Takahashi, Y. K., Igarashi, K. M., & Yamaguchi, M. (2006). Maps of odorant molecular features in the Mammalian olfactory bulb. *Physiological Reviews, 86*, 409–433.

Mombaerts, P. (1996). Targeting olfaction. *Current Opinion in Neurobiology, 6*, 481–486.

Pinato, G., & Midtgaard, J. (2004). Dendritic sodium spikelets and low-threshold calcium spikes in turtle olfactory bulb granule cells. *Journal of Neurophysiology, 93*, 1285–1294.

Rall, W., & Shepherd, G. M. (1968). Theoretical reconstruction of field potentials and dendrodendritic synaptic interactions in olfactory bulb. *Journal of Neurophysiology, 31*, 884–915.

Rall, W., Shepherd, G. M., Reese, T. S., & Brightman, M. W. (1966). Dendrodendritic synaptic pathway for inhibition in the olfactory bulb. *Experimental Neurology, 14*, 44–56.

Ressler, K. J., Sullivan, S. L., & Buck, L. B. (1994). Information coding in the olfactory system: Evidence for a stereotyped and highly organized epitope map in the olfactory bulb. *Cell, 79*, 1245–1255.

Schoppa, N. E., Kinzie, J. M., Sahara, Y., Segerson, T. P., & Westbrook, G. L. (1998). Dendrodendritic inhibition in the olfactory bulb is driven by NMDA receptors. *Journal of Neuroscience, 18*, 6790–6802.

Schoppa, N. E., & Westbrook, G. L. (1999). Regulation of synaptic timing in the olfactory bulb by an A-type potassium current. *Nature Neuroscience, 2*, 1106–1113.

Shepherd, G. M., & Brayton, R. K. (1979). Computer simulation of a dendrodendritic synaptic circuit for self- and lateral-inhibition in the olfactory bulb. *Brain Research, 175*, 377–382.

Shepherd, G. M., & Greer, C. A. (1998). Olfactory bulb. In G. M. Shepherd (Ed.), *The synaptic organization of the brain*. New York: Oxford University Press, p. 170.

Uchida, N., & Mainen, Z. F. (2003). Speed and accuracy of olfactory discrimination in the rat. *Nature Neuroscience, 6*, 1224–1229.

Urban, N. N., & Sakmann, B. (2002). Reciprocal intraglomerular excitation and intra- and interglomerular lateral inhibition between mouse olfactory bulb mitral cells. *Journal of Physiology, 542*, 355–367.

Vassar, R., Chao, S. K., Sitcheran, R., Nunez, J. M., Vosshall, L. B., & Axel, R. (1994). Topographic organization of sensory projections to the olfactory bulb. *Cell, 79*, 981–991.

Wellis, D. P., & Kauer, J. S. (1994). GABAergic and glutamatergic synaptic input to identified granule cells in salamander olfactory bulb. *Journal of Physiology, 475*, 419–430.

Willhite, D. C., Nguyen, K. T., Masurkar, A. V., Greer, C. A., Shepherd, G. M., & Chen, W. R. (2006). Viral tracing identifies distributed columnar organization in the olfactory bulb. *Proceedings of the National Academy of Sciences of the United States of America, 103*, 12592–12597.

Woolf, T. B., Shepherd, G. M., & Greer, C. A. (1991). Local information processing in dendritic trees: Subsets of spines in granule cells of the mammalian olfactory bulb. *Journal of Neuroscience, 11*, 1837–1854.

Xiong, W., & Chen, W. R. (2002). Dynamic gating of spike propagation in the mitral cell lateral dendrites. *Neuron, 34*, 115–126.

Xu, F. Q., Liu, N., Kida, I., Rothman, D. L., Hyder, F., & Shepherd, G. M. (2003). Odor maps of aldehydes and esters revealed by fMRI in the glomerular layer of the mouse olfactory bulb. *Proceedings of the National Academy of Sciences of the United States of America, 100*, 11029–11034.

Yokoi, M., Mori, K., & Nakanishi, S. (1995). Refinement of odor molecule tuning by dendrodendritic synaptic inhibition in the olfactory bulb. *Proceedings of the National Academy of Sciences of the United States of America, 92*, 3371–3375.

Zelles, Y., Boyd, J. D., Hardy, A. B., & Delaney, K. R. (2006). Branch-specific Ca^{2+} influx from Na^+-dependent dendritic spikes in olfactory granule cells. *Journal of Neuroscience, 26*, 30–40.